Petroleum and Coal

Article **Open Access**

Reservoir Volume Risk Estimation from 3D Seismic and Well Logs – A Multiple-Point Stochastic Inversion Application Case Study

Dele Falebita[1], Adeniyi Olusanya[1] Timothy Tella[2]*

[1] *Department of Geology, Obafemi Awolowo University, Ile-Ife, Nigeria*
[2] *Institute of Geosciences, University of Potsdam, Potsdam, Germany*

Received October 26, 2022; Accepted April 3, 2023

Abstract

This study assesses reservoir volume risk from a combination of well logs and seismic volume using multiple-point stochastic inversion technique. This inversion procedure allows for a fast and cost-effective means of transforming seismic reflection to rock properties for reservoir modelling and risk analysis. The stochastically quantified reservoir parameters necessary for volume estimation are based on probability distribution and so assess the risks associated with the hydrocarbon volume and potential extraction plan. This study, therefore, showcases the application of this inversion technique and confirms the integral role of stochastic simulation in reservoir volume prediction, estimation, quantification and risk analysis.

Keywords: *Reservoir risk; Volume estimation; Multiple-point; Stochastic inversion.*

1. Introduction

Seismic inversion has found a place as a critical tool for reservoir characterization. This is because it allows for the transformation of seismic reflection data into rock properties (impedance) [1-2]. It is often applied to refine the quality and consistency of data in order to robustly aid the estimation and prediction of rock properties [3-4]. Stochastic seismic inversion integrates spatially correlated properties obtained from seismic and log data for reservoir modelling and uncertainty analysis [2]. The seismic data, which has contributed significantly to hydrocarbon exploration [5-8] provides quality lateral resolution while the log data provides quality vertical resolution for the inversion process [1,9]. This process allows for the generation of multiple equally probable representations of the unknown reservoir property thereby quantifying associated uncertainty.

Multiple-point geostatistics refers to the statistics of the same variable at several locations. The procedure has been applied by using training image as a-priori geological model to capture the essential characteristics of reservoirs [10-13]. The delineated characteristics from the training image(s) are then tied to specific reservoir location. This leads to several realizations of the unknown realities of the reservoir characteristics which can be used to quantify risk. There is also the impedance approach [14] that requires picked horizons, well logs, impedance model, estimated seismic wavelet and seismic data. This procedure is compiled as a multiple-point stochastic inversion (MPSI) plugin to Opendtect™. It is a fast, model-based stochastic seismic inversion structure that uses fast Fourier transform (FFT) algorithms to simulate impedance realizations, which are then tied to the seismic amplitude and well impedance data [15-17].

This impedance approach was adopted in this study, where the MPSI technique was applied to estimate reservoir volume risk from structural and stratigraphic patterns obtained from 3D seismic and well log data. The process involves the estimation of lateral continuity of hydrocarbon reservoir properties, and quantification of associated uncertainties to guide optimal hydrocarbon extraction decision making. Structural and stratigraphic patterns are major factors that affect reservoir connectivity and volume risk which in turn influence fluid flow characteristics in hydrocarbons reservoirs. Structural patterns (e.g., tops and thickness of reservoirs) are easily picked on conventional seismic section while stratigraphic patterns - internal rock characteristics (e.g. lithology, porosity and fluid type) are better interpreted from inverted data [2].

2. The region of study

The regional geology of the study area is that of the Niger delta petroleum province in the southern part of Nigeria. The delta was formed as a result of the break-up of the African plate from the South American plate [18-20]. There are three major stratigraphic sequences of the Tertiary sediments deposited in the delta through time. They are the prodelta Akata shale, the paralic Agbada formation and the unconsolidated Benin sand (Fig. 1). The Akata shale age ranges from Eocene to Recent and it is the main hydrocarbon source rock. It is continuous in the subsurface and defines the base of the delta [18, 21]. The Agbada formation is the main target for hydrocarbon exploration. It is a marine sand-shale sequence with age between Lower Eocene and Pleistocene. The Benin sand is the youngest and mostly continental in origin. Its age is between Eocene and Recent and occurs throughout the delta [21]. There is an interplay of structure and stratigraphy which in turn, is influenced by the adjustment of underlying shale to the weight of the overlying sediments [18]. This assists in the formation of the commonly observed syn-sedimentary faults and roll-over structures [22]. Regional sand pinch outs and truncations as well as palaeo-channel fills are among the common stratigraphic traps present where the transgressive marine shales of the Agbada Formation form the major regional top seals.

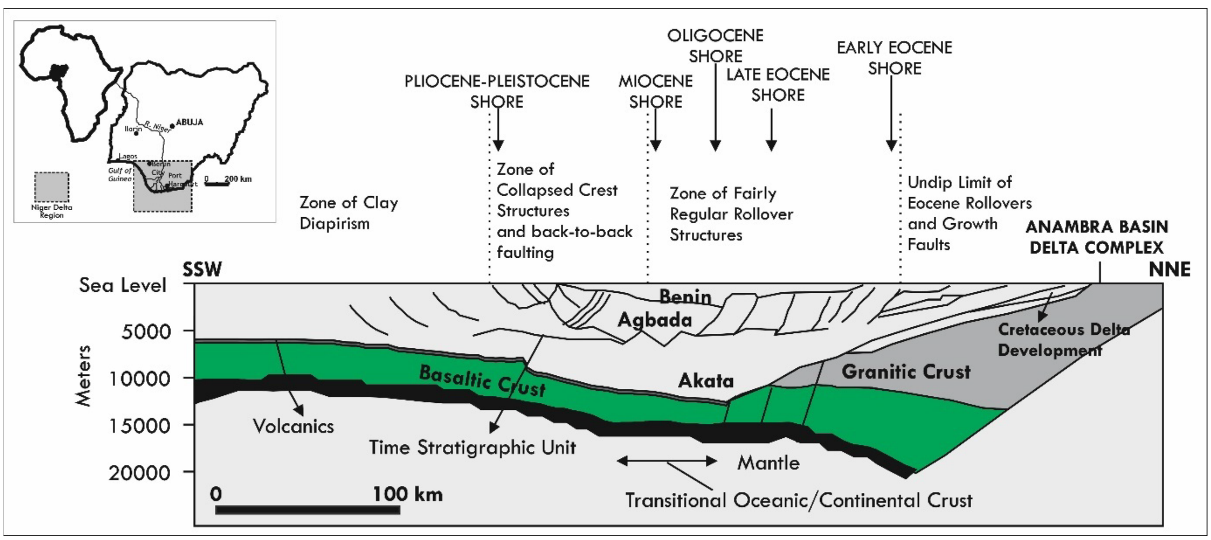

Figure 1. Structuration of the Niger delta region (modified after [29])

3. Stochastic inversion workflow

The stochastic inversion workflow was carried out using the multiple-point stochastic inversion (MPSI) plugin of the Opendtect software following the steps described in Figure 2 with each step requiring input from the previous step. The plugin makes use of fast, robust and low-cost processes that model a full seismic bandwidth [15-17,23,25] which is based on seismic inversion technology [1].

The first step is to produce 3D impedance model constrained by a variogram of specific range and sill. The 3D impedance model is constructed from picked horizons and well data. A variogram is a tool that investigates and quantifies the spatial variability of the parameter of interest and serves as critical input in geostatistical estimation and simulation algorithms [24]. It measures the average dissimilarity between sample points at a displacement vector (h) from each other. Its value increases as samples become more dissimilar. For a pair of sample points, it is simplified as:

$$2\gamma(h) = \frac{1}{N(h)} \sum_{\propto=1}^{N(h)} \langle z(u_{\propto}) - z(u_{\propto} + h) \rangle^2 \qquad 1$$

where $2\gamma(h)$ = variogram; $N(h)$ = the number of sample pairs in a lag interval; u_α = the vector of spatial coordinates of the αth individual; $z(u_\alpha)$ and $z(u_\alpha+h)$ are values of the attribute at two points at an interval displacement vector (h) [25].

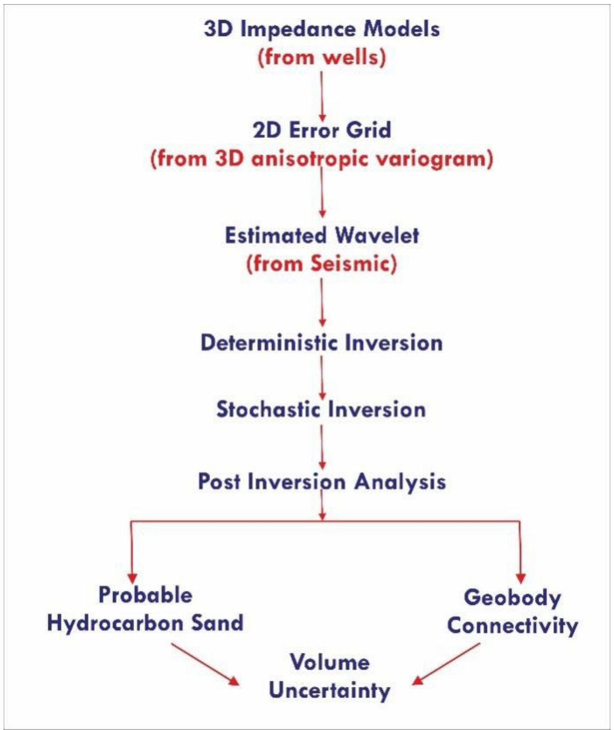

Figure 2. The stochastic workflow

The second step is the 2D quantification of the geostatistical standard deviation (referred to as error grid) of attribute relative to the well locations. This provides a spatial control on the inversion convergence factors and makes sure the impedance model is anchored to data from well at a close range while allowing contributions from the seismic data away from the well locations [15-17, 23]. The third step is to generate the deterministic inversion model which requires an estimated wavelet. A deterministic model associates to any unsampled location (u), a single estimated value, taken as the true value such that error is assumed to be negligible. The fourth step is the stochastic inversion. A stochastic inversion provides a set of possible values with the corresponding probabilities of occurrence [27-28]. Such representations reflect the risk associated with the unknown value z(u) [27-28]. Stochastic inversion can be computed at a reservoir scale, it removes tuning effect and can be used to monitor reservoir connectivity [2]. The post inversion analysis is the last step and it is done to make sense of the inversion results.

4. Results and discussion

4.1. Basic characteristics of the hydrocarbon-bearing sands

Table 1 summarizes the petrophysical parameters of the three hydrocarbon sands delineated from the well logs. Sand A is the shallowest while Sand C is the deepest. The average subsea (SS) depth of Sand A is 2905.85 m; depth of Sand B is 3237.3 while that of Sand C is 3389.73. In Sand A, the average gross pay (GROSS) is 21.48 m; net-to-gross (NGR) is 0.01; porosity (PHA) is 32% and hydrocarbon saturation (SH) is 79%. In Sand B, the average gross pay is 24.30 m; net-to-gross is 0.07; porosity is 27% and hydrocarbon saturation is 77%. In Sand C, the average gross pay is 40.93 m; net-to-gross is 0.14; porosity is 27% and hydrocarbon saturation is 83%. It appears that Sand C has the best hydrocarbon properties of the three sands. Figure 3 is a stratigraphic correlation from six wells indicating the relative positions of the sands and some faults with depth. Wells TW-03 and TW-06 are deviated wells while the remaining four wells – TW-02, TW-05, TW-01 and TW-04 are straight holes.

Table 1. The Petrophysical properties of the sands

Sand	Depth Sub-sea (m)	GROSS (m)	NGR	PHA	SHD
A	-2905.85	21.48	0.01	0.32	0.79
B	-3237.30	24.30	0.07	0.27	0.77
C	-3389.73	40.93	0.14	0.27	0.83
Average		28.90333	0.073333	0.286667	0.796667
Standard deviation		10.51041	0.065064	0.028868	0.030551

GROSS = Gross pay, NGR = net-to-gross ratio, PHA = porosity, SHD = hydrocarbon saturation

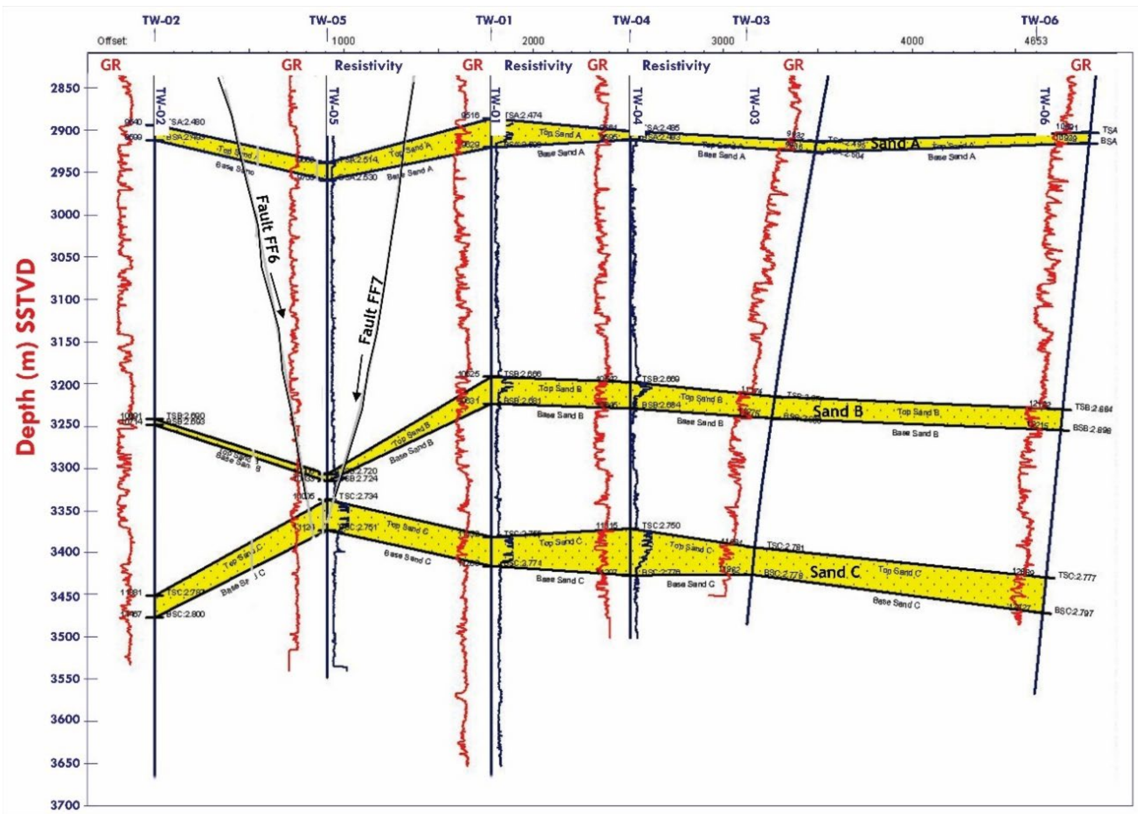

Figure 3. Stratigraphic correlation of the hydrocarbon sands

4.2. The 3D impedance models

The zone of interest for the 3D impedance modelling is constrained between 2000 ms and 3200 ms of the seismic volume. This is defined by two picked horizons, namely TH-01 as the upper boundary and TH-02 is the lower boundary. TH-01 approximates the top of Sand A while TH-02 approximates the base of Sand C. Figure 4, is a 3D view of the relative positions of the horizons and the wells that penetrate them within the time interval. This interval bounds the three hydrocarbon bearing sands as indicated in Figure 3. The 3D broadband impedance model (Fig. 5) was produced from the combination of the velocity obtained from the sonic log as well as the density from the density log with the two horizons and the 3D seismic volume. The gridding was constrained by 3D anisotropic exponential variogram with representative two horizontal (X and Y) ranges of 2500 m and vertical range in the Z-direction as 25 ms. The exponential variogram function is defined mathematically by a range (a) and sill (c) (*see Equation 2*) and represents a coarse spatial behaviour [23] typical of geological scenario.

$$\gamma(h) = c\left[1 - e^{\left(-\frac{3h}{a}\right)}\right] \qquad 2$$

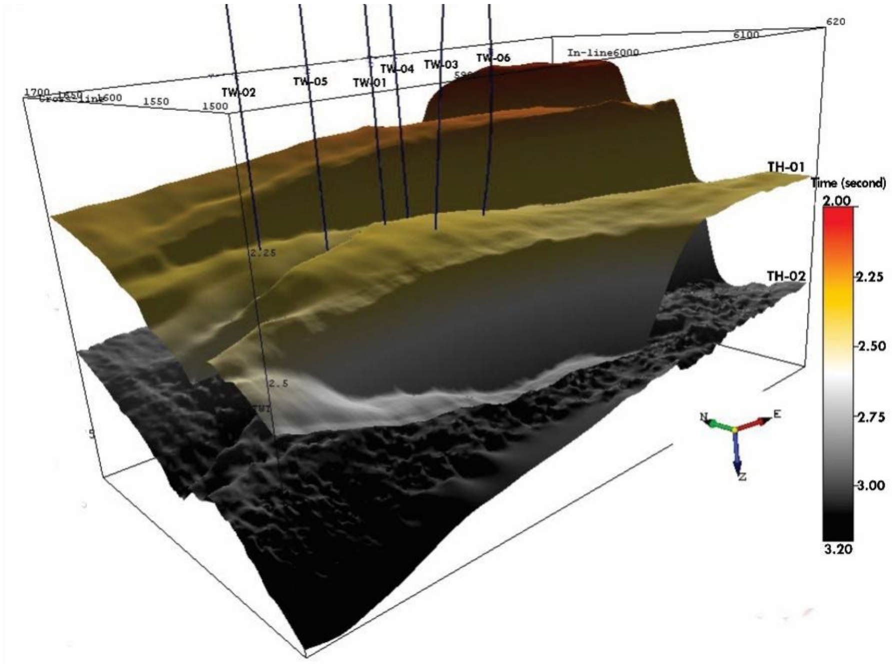

Figure 4. 3D view of the horizons (tops of formations) and the wells

The 3D impedance model (Fig.5) shows a representative well TW-01 penetrating distinct bands (layers) of impedance values ranging between 17000 and 30000 ms^{-1} x gcm^{-3}. On the left side of the well is the gamma ray (GR) log while on the right side is the deep resistivity (RES) log. The GR gives indication of the sand-shale lithology while the resistivity gives indication of the hydrocarbon presence. The very high impedance intervals can easily be identified or isolated within the model. Broadly, it seems that the impedance increases with depth and the hydrocarbon sands (i.e., Sand A, Sand B, and Sand C) are associated with higher impedance (generally above 20000 ms^{-1} x gcm^{-3}).

4.3. The deterministic inversion model

The deterministic inversion makes use of the (1) seismic volume, (2) 3D impedance models (3) a 2D error grid and (4) an estimated wavelet. The 3D impedance model serves as a priori geologic information while the 2D Error grid (Fig. 6) provides a spatial control by making sure the impedance model has more of well control near the wells relative to seismic control away from the wells. The 2D error grid was generated using the 3D impedance model and the exponential variogram type within 2000 m radius of influence around the wells. The estimated wavelet helps in the conversion of reflectivity at the well to seismic trace where a natural logarithm is applied to correct for any exponential relation between the impedance and reflectivity. The deterministic inversion represents the expected value of the average of several realizations (Fig. 7). The impedance ranges between 17000 and 37000 ms^{-1} x gcm^{-3} and displays more variability/rugosity on the sections than the initial 3D impedance model (Fig. 5). Moreover, identified hydrocarbon sands are still associated with higher impedance values.

4.4. Stochastic inversion models

The stochastic inversion uses a fast Fourier transform (FFT) procedure on the combined inputs of the original seismic volume, initial 3D impedance model, error grid, and deterministic inversion model to generate impedance realizations which are then tied to seismic amplitude and well data [15-17,23,26]. It involves the normal score (forward) and inverse normal score (backward) transformations respectively, of the impedance values obtained from the wells in the frequency domain. The realizations obtained from the stochastic inversion allow for the assessment of risk associated with the reservoir properties [2]. Figure 8 shows the twenty realizations of the impedance models generated by the process. The realizations have observable changing and differing variabilities which can be used to quantify the risk associated with the modelling process compared to the only deterministic inversion model of Figure 7. The impedance values range between 11000 and 58000 ms^{-1} x gcm^{-3} and confirm the non-uniqueness of the inversion solution. This is because a number of impedance solutions would give a representative match to the seismic trace when the reflection coefficient is convolved with a wavelet.

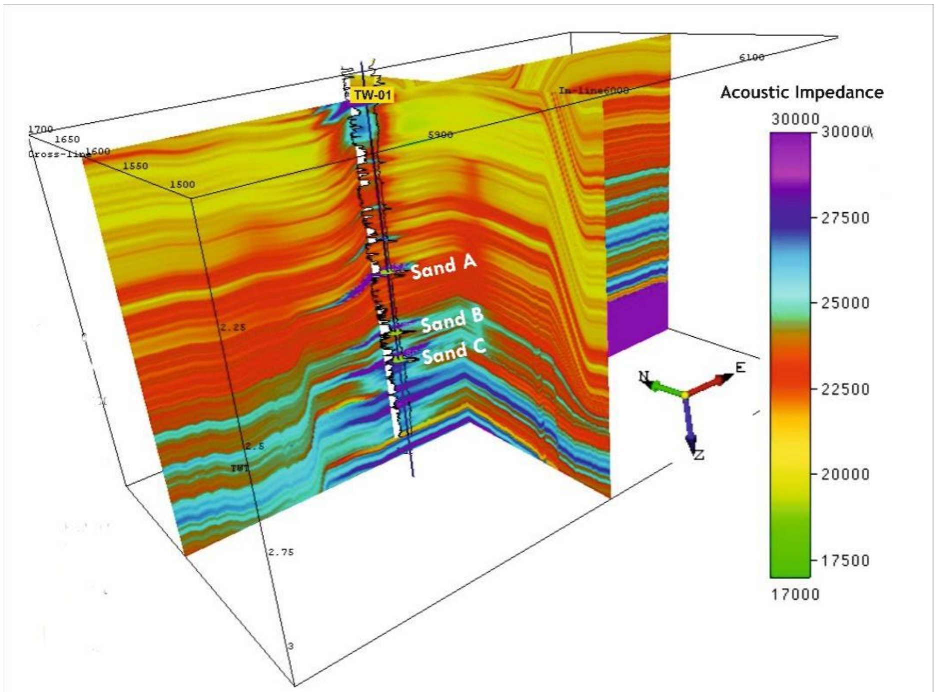

Figure 5. 3D impedance model

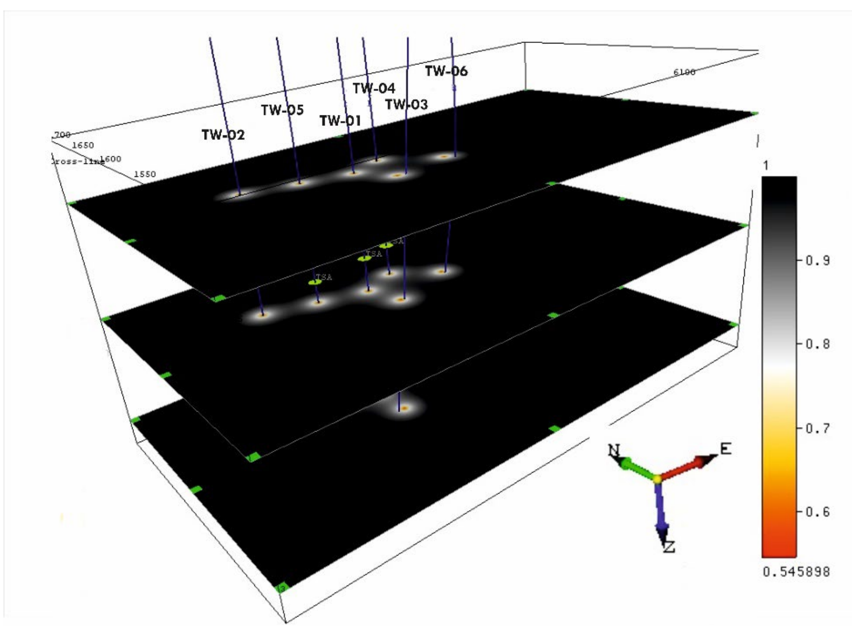

Figure 6. 2D Error grid

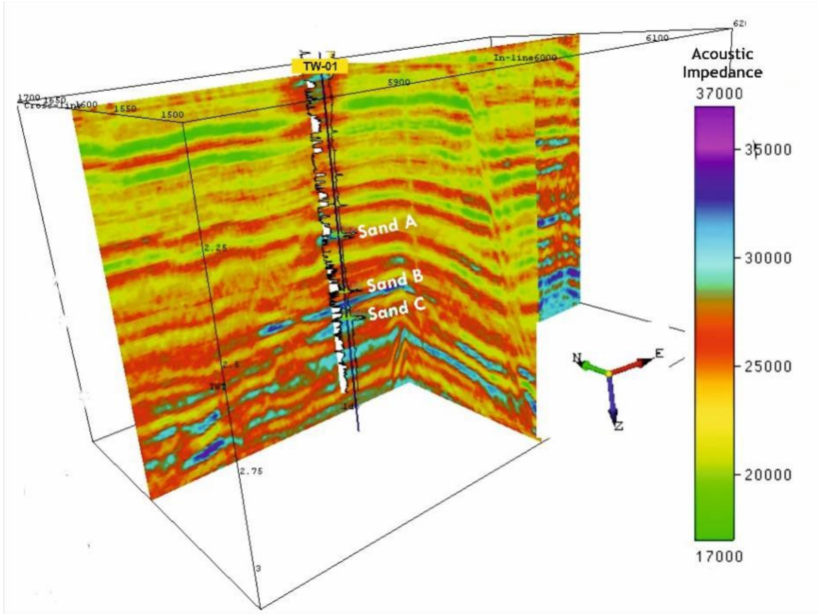

Figure 7. Deterministic inversion model

4.5. Post-inversion analysis

4.5.1. Probable hydrocarbon sand

Figure 9 is the result of the probability of the occurrence of hydrocarbon sands based on the number of times at which each realization gives an impedance value between 23000 and 50000 ms^{-1} x gcm^{-3}. This range represents the threshold interval for the occurrence of the hydrocarbon sands within the cube (see Fig. 5). Fig. 9a represents probability distribution within the seismic volume while 9b is the annotated probability on crossline 1615. The section shows the wells (TW-05, TW-01 and TW-04) as well as the gamma ray (left log) and resistivity (right log). The sands are also indicated as TSA – Sand A; TSB – Sand B and TSC – Sand C respectively. The probability is maximum at 1 (pink colour) and minimum at 0 (blue colour). The output of the probability is the chance of success and therefore a measure of the risk in predicting the outcome. It appears that the probability for the occurrence of hydrocarbon sands is highest at depth interval within which Sands B and C are found relative to Sand A.

4.5.2. Geobody connectivity

A geobody is a group of cells having similar properties which can indicate the presence of a particular rock type or fluid phase. It is usually identified by an integer greater than 0, where 0 represents a background matrix. In this study, geobodies are identified by scanning the nodes of each realization and mark those nodes that are connected to an initial seed within an impedance range. The initially connected seeds are then used as additional seed points for further scanning. The twenty stochastic realizations (Fig. 8) were analyzed for geobody connectivity within the impedance range of 23000 and 50000 ms^{-1} x gcm^{-3}. The twenty geobody realizations are presented as Figure 10. Each realization is interpreted as a plausible representation of a 3D structurally- and stratigraphically-controlled clusters of connected geobodies. The probability of connectedness increases from 0 (blue) to pink (1). Figure 11 is a collection of twenty vertical sections through crossline 1615 of the twenty geobody realizations. They show the different variabilities of the realizations and in most cases, the hydrocarbon reservoirs TSB (Sand B) and TSC (Sand C) are much more associated with connected geobodies than TSA (Sand A). They also point to the risk associated with the potential hydrocarbon flow, volume and reserves uncertainty within the interval and confirm that subsurface interconnectedness should never be represented by layer-cake models. A combination of intervals with higher probability of connectivity (Fig. 10) and presence of hydrocarbon (Fig. 9) are realistic targets for further exploitation.

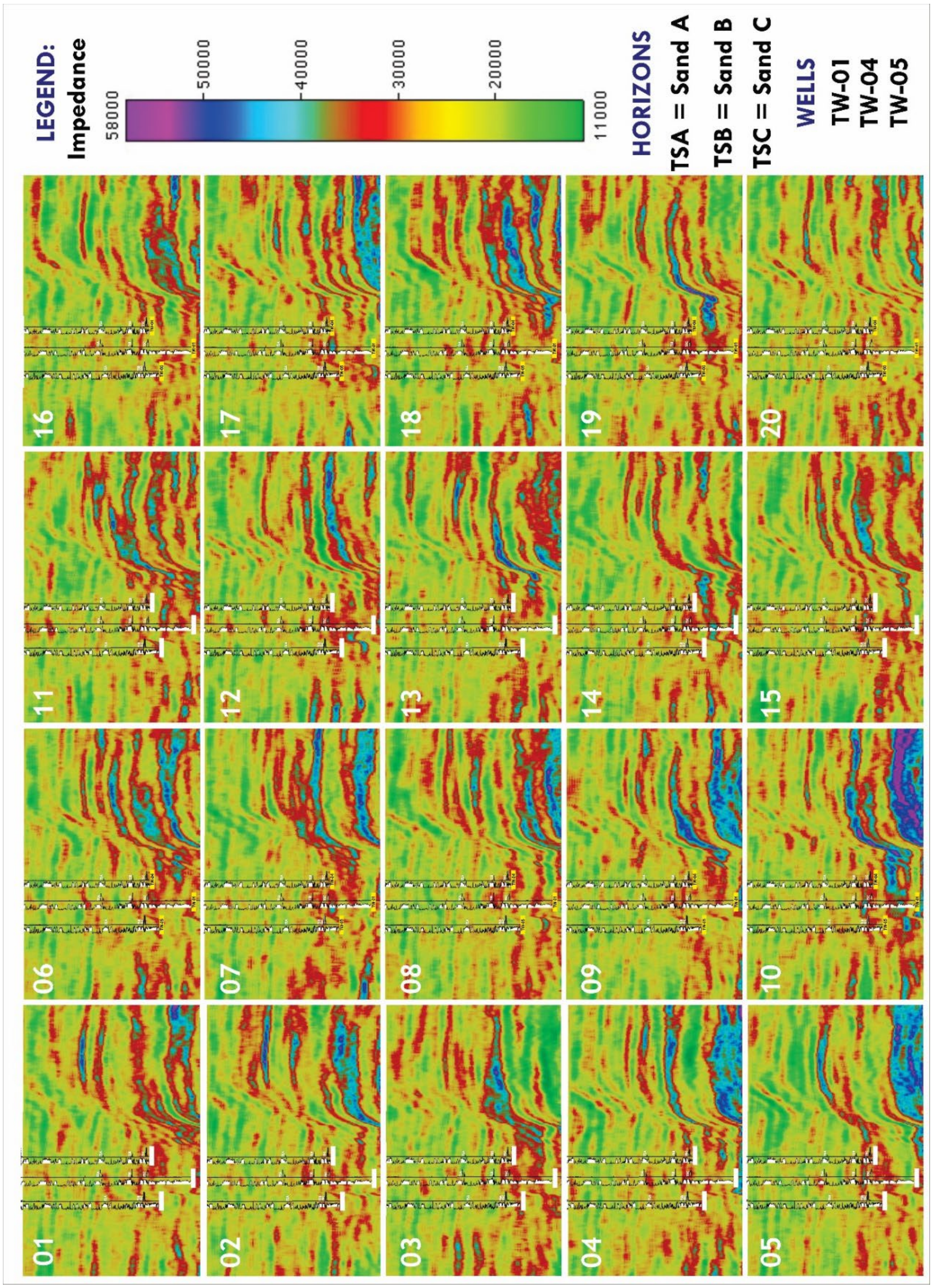

Figure 8. Twenty realizations of the impedance models.

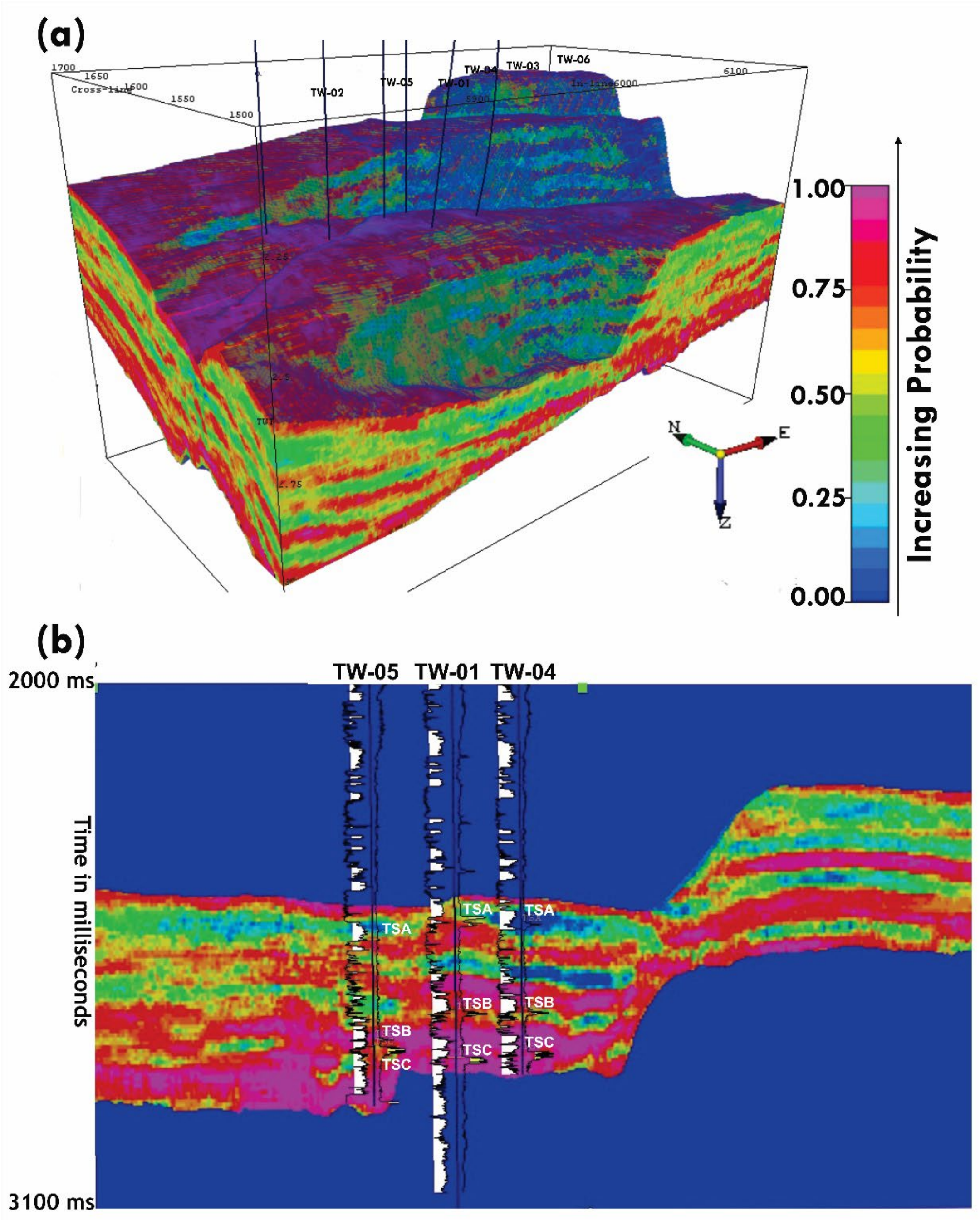

Figure 9. (a) 3D view of probable distribution of hydrocarbon sands (b) A sectional view of the probable distribution of hydrocarbon sands on crossline 1615

4.5.3. Volume risk

Table 2 is a summary of the three main parameters derived from each geobody connectivity realization. There is the total area formed by the connected cells in square metres, the average thickness of the interval defined by the top horizon TH-01 and bottom horizon TH-02 in metres and the gross connected volume in cubic metres which is the multiplication of the connected area by the average thickness of the interval. The connected area varies between 88242 and 88621 square metres; average thickness varies from 147.3786 to 223.6568 m, while the gross connected volume varies between about 13.0 and 19.8 million cubic metres (mcm)– a difference of about 6.8 (mcm).

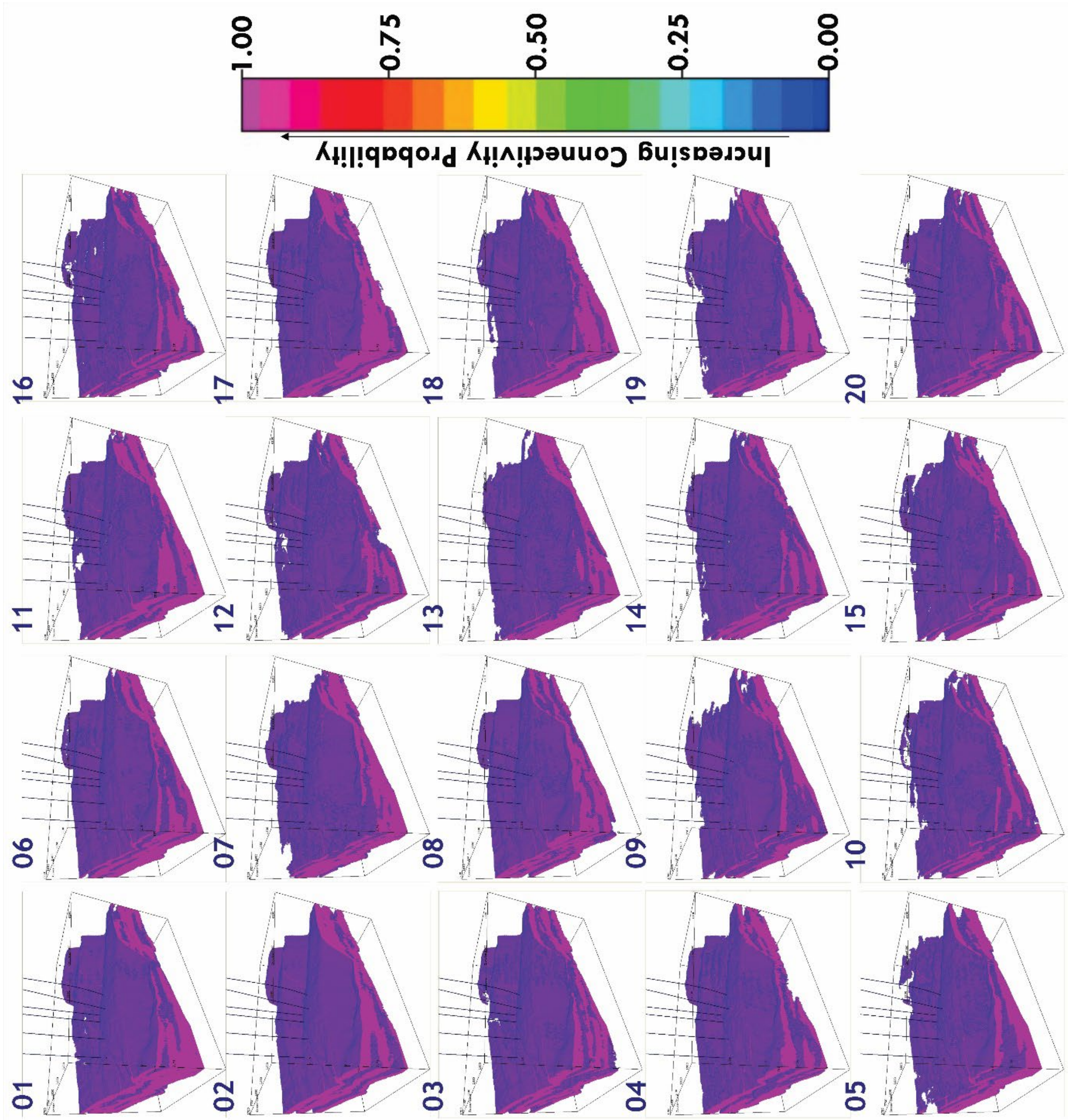

Figure 10. Twenty realizations of 3D view of geobody connectivity

The volume risk modelling was performed by making use of normal inverse function (equation 3) on each parameter of GROSS, NGR, PHA and SHD. The function returns an equally probable random number Y, specified by a random number generator RAND() within a probability range of 0 and 1 for a given average (μ) and standard deviation (σ) value.

=NORMINV(RAND(), μ , σ) 3

The average and standard deviation values of the connected gross volume (Table 2) are derived from the seismic volume. While the average and standard deviation values of NGR, PHA and SHD (Table 1) are derived from well logs. These values serve as inputs into the subsequent volume risk modeling.

For each parameter (GROSS, NGR, PHA and SHD), one thousand equally probable random numbers were simulated for which uncertainties were determined from the subsequently plotted cumulative distribution functions (Figs 12a, b, c, d) at five (5) risk levels, namely P10, P25, P50, P75 and P90. These risk levels are interpreted in terms of probability of obtaining more or less than a specified value. In other words, for the specified value, after 1000 runs, P10 is 90% chance of obtaining more; P25 represents 75% chance of obtaining more; P50 means equal chance of obtaining more or less (the median); P75 represents 25% chance of obtaining more while P90 has 10% of obtaining more.

Table 3 is the statistics of the parameters at the specified risk levels. At P90, there is only a 10% chance of having more than 18.9 million cubic metres of gross connected volume; 0.16 of net-to-gross; 33% of average porosity and 83% of hydrocarbon saturation. Conversely, at P10, there is a 90% chance of obtaining more than 13.9 million cubic metres of gross connected volume; 10^{-5} of net-to-gross; 25% of average porosity and 76% of hydrocarbon saturation. At P50, there is a 50-50 (equal) chance of obtaining more or less than 16.5 million cubic metres of gross connected volume; 0.08 of net-to-gross; 29% of average porosity and 80% of hydrocarbon saturation. At P25, there is a 75% chance of obtaining more than 15.3 million cubic metre of gross connected; 0.03 of net-to-gross; 27% of average porosity and 78% of hydrocarbon saturation. Whereas at P75, there is only a 25% chance of obtaining more than 17.8 million cubic metre of gross connected volume; 0.13 of net-to-gross; 31% of porosity and 82% of hydrocarbon saturation.

Table 2. Geobody connectivity and volume statistics for the twenty realizations

Realization	Connected (area, m^2)	Thickness (m)	Connected gross volume (m^3)
1	88604	215.7658	19,117,712.94
2	88621	223.6568	19,820,689.27
3	88616	186.8935	16,561,754.40
4	88609	189.4393	16,786,026.93
5	88621	178.6394	15,831,202.27
6	88621	210.7657	18,678,267.10
7	88621	213.6817	18,936,685.94
8	88618	192.0880	17,022,454.38
9	88620	166.8064	14,782,383.17
10	88571	153.7869	13,621,059.52
11	88619	205.0680	18,172,921.09
12	88421	168.3806	14,888,381.03
13	88620	177.4458	15,725,246.80
14	88534	170.0692	15,056,906.55
15	88621	156.4782	13,867,254.56
16	88242	147.3786	13,004,982.42
17	88352	197.5424	17,453,266.12
18	88384	200.0518	17,681,378.29
19	88611	185.9834	16,480,175.06
20	88615	183.4497	16,256,395.17
		Average	16,499,407.78
		Standard deviation	1,922,062.52

Table 3. Statistics of parameters at the P10, P25, P50, P75 and P90 risk levels

RISK	GROSS (m^3)	NTG	PHA	SHD
90	18,940,000	0.16000	0.33	0.83
75	17,770,000	0.13000	0.31	0.82
50	16,550,000	0.08000	0.29	0.80
25	15,260,000	0.03000	0.27	0.78
10	13,970,000	0.00001	0.25	0.76

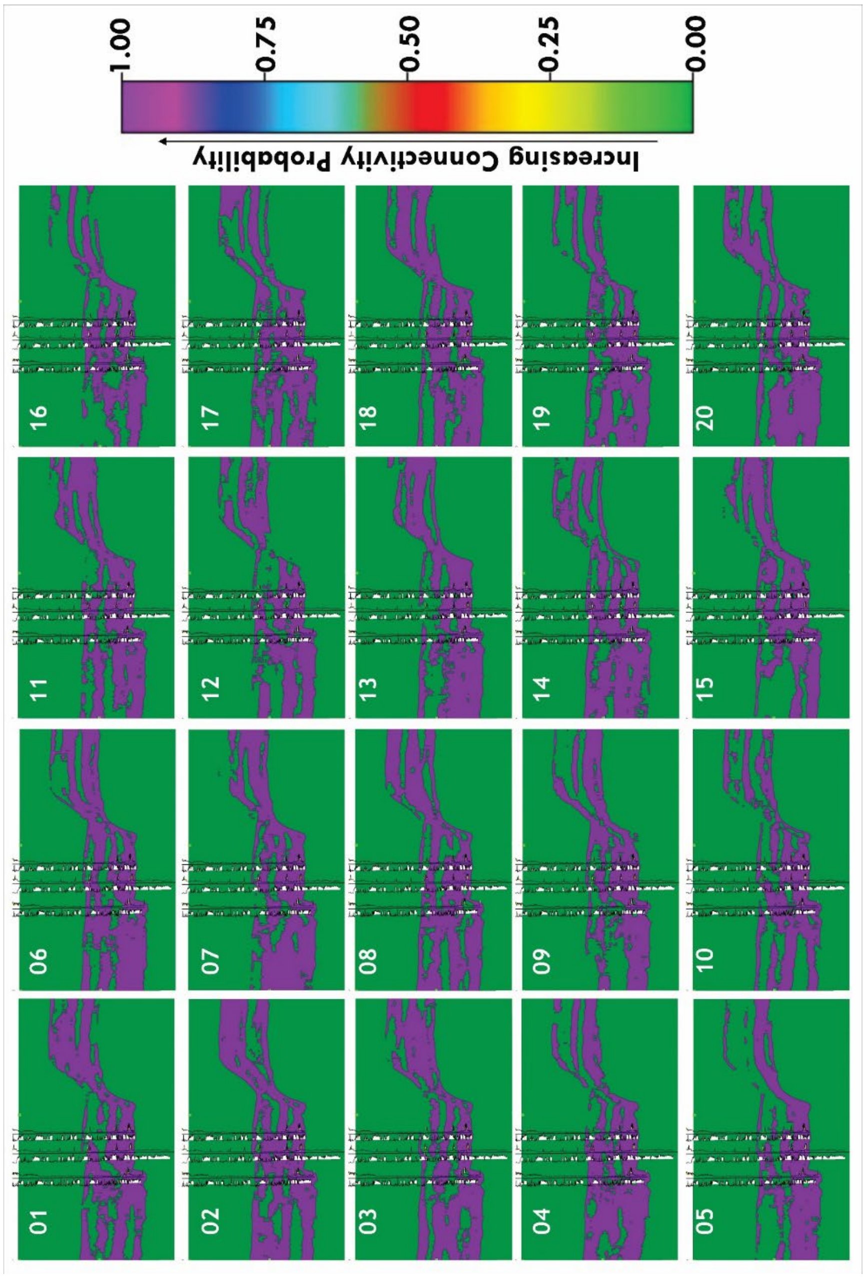

Figure 11. A sectional view of the connectivity on crossline 1615 from each of the twenty geobody realizations

The quantified values of these parameters at the five risk levels (Table 3) serve as inputs into the computation of probable hydrocarbon in place (HIP) in cubic metres. Hydrocarbon in place is given by equation 4 excluding barrel or gas conversion and formation volume factors. The ratio of barrel or gas conversion and formation volume factors gives a constant that can be used to multiply equation 4 whenever available.

HIP = GROSS * NTG *PHA*SHD (4)

However, instead of multiplying the factors directly to get only five HIP results at different risk levels as given in Table 3, we adopted a cross-combination of factors to deep-learn other possibilities between as based on Figure 13. Each parameter at a probability level is allowed to combine with other parameters at different probability levels. This is so, because the combination of the parameters may not be limited to the same probability level. As a result of this, six hundred and twenty-five (625) HIP results were calculated instead of just five (5) resulting in Tables 4-8. If the parameters in Table 3 had been multiplied directly at each probability level, the hydrocarbon volume obtained would just be a volume (boldened) out of 125 possibilities per probability level (Tables 4-8).

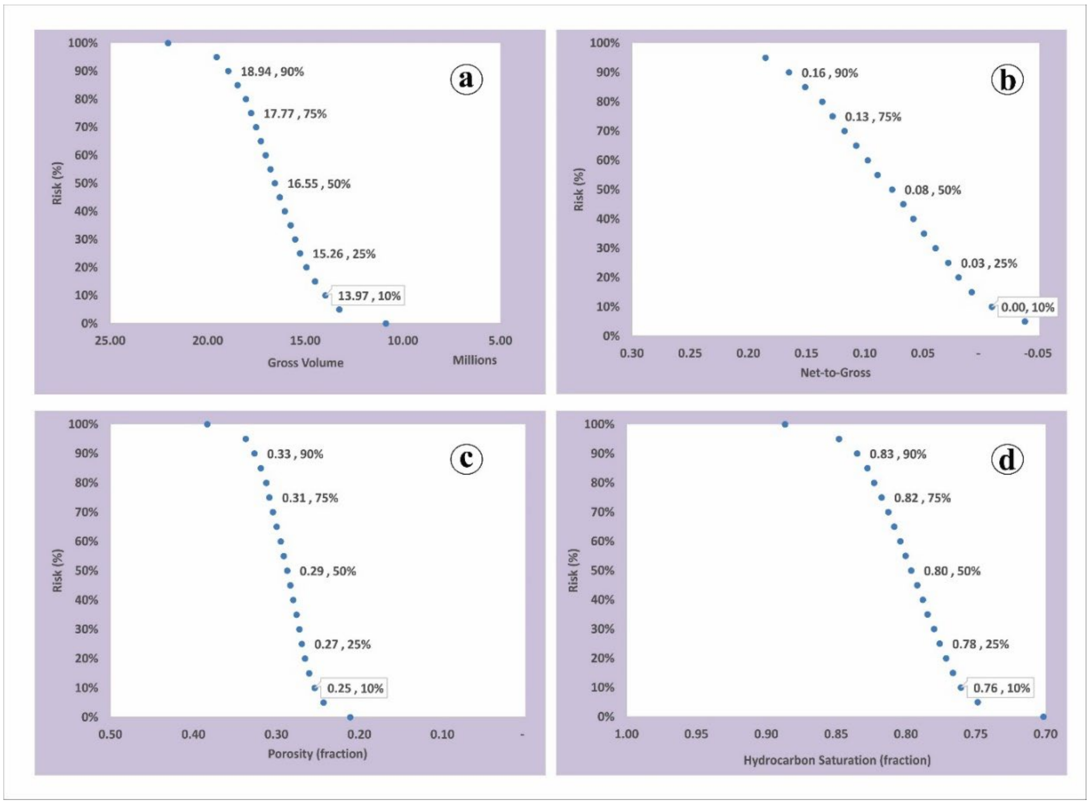

Figure 12. The cumulative distribution functions (CDFs) of the four parameters

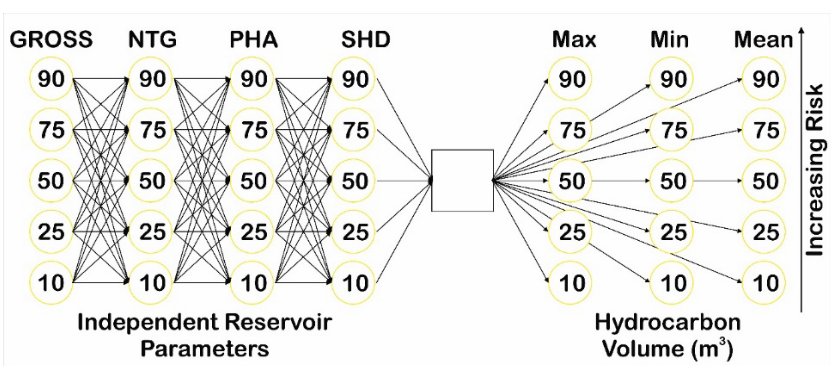

Figure 13. Cross-combination of parameters at different probability levels

Table 4. Risked volume at P90

Risk	90	75	50	25	10
90	816,291.84	790,782.72	739,764.48	688,746.24	637,728.00
75	796,856.32	771,954.56	722,151.04	672,347.52	622,544.00
50	777,420.80	753,126.40	704,537.60	655,948.80	607,360.00
25	757,985.28	734,298.24	686,924.16	639,550.08	592,176.00
10	738,549.76	715,470.08	669,310.72	623,151.36	576,992.00
90	612,218.88	593,087.04	554,823.36	516,559.68	478,296.00
75	597,642.24	578,965.92	541,613.28	504,260.64	466,908.00
50	583,065.60	564,844.80	528,403.20	491,961.60	455,520.00
25	568,488.96	550,723.68	515,193.12	479,662.56	444,132.00
10	553,912.32	536,602.56	501,983.04	467,363.52	432,744.00
90	408,145.92	395,391.36	369,882.24	344,373.12	318,864.00
75	398,428.16	385,977.28	361,075.52	336,173.76	311,272.00
50	388,710.40	376,563.20	352,268.80	327,974.40	303,680.00
25	378,992.64	367,149.12	343,462.08	319,775.04	296,088.00
10	369,274.88	357,735.04	334,655.36	311,575.68	288,496.00
90	153,054.72	148,271.76	138,705.84	129,139.92	119,574.00
75	149,410.56	144,741.48	135,403.32	126,065.16	116,727.00
50	145,766.40	141,211.20	132,100.80	122,990.40	113,880.00
25	142,122.24	137,680.92	128,798.28	119,915.64	111,033.00
10	138,478.08	134,150.64	125,495.76	116,840.88	108,186.00
90	51.02	49.42	46.24	43.05	39.86
75	49.80	48.25	45.13	42.02	38.91
50	48.59	47.07	44.03	41.00	37.96
25	47.37	45.89	42.93	39.97	37.01
10	46.16	44.72	41.83	38.95	36.06

Table 5. Risked volume at P75

Risk	90	75	50	25	10
90	760,381.44	736,619.52	689,095.68	641,571.84	594,048.00
75	742,277.12	719,080.96	672,688.64	626,296.32	579,904.00
50	724,172.80	701,542.40	656,281.60	611,020.80	565,760.00
25	706,068.48	684,003.84	639,874.56	595,745.28	551,616.00
10	687,964.16	666,465.28	623,467.52	580,469.76	537,472.00
90	570,286.08	552,464.64	516,821.76	481,178.88	445,536.00
75	556,707.84	539,310.72	504,516.48	469,722.24	434,928.00
50	543,129.60	526,156.80	492,211.20	458,265.60	424,320.00
25	529,551.36	513,002.88	479,905.92	446,808.96	413,712.00
10	515,973.12	499,848.96	467,600.64	435,352.32	403,104.00
90	380,190.72	368,309.76	344,547.84	320,785.92	297,024.00
75	371,138.56	359,540.48	336,344.32	313,148.16	289,952.00
50	362,086.40	350,771.20	328,140.80	305,510.40	282,880.00
25	353,034.24	342,001.92	319,937.28	297,872.64	275,808.00
10	343,982.08	333,232.64	311,733.76	290,234.88	268,736.00
90	142,571.52	138,116.16	129,205.44	120,294.72	111,384.00
75	139,176.96	134,827.68	126,129.12	117,430.56	108,732.00
50	135,782.40	131,539.20	123,052.80	114,566.40	106,080.00
25	132,387.84	128,250.72	119,976.48	111,702.24	103,428.00
10	128,993.28	124,962.24	116,900.16	108,838.08	100,776.00
90	47.52	46.04	43.07	40.10	37.13
75	46.39	44.94	42.04	39.14	36.24
50	45.26	43.85	41.02	38.19	35.36
25	44.13	42.75	39.99	37.23	34.48
10	43.00	41.65	38.97	36.28	33.59

Table 6. Risked volume at P50

Risk	90	75	50	25	10
90	705,331.20	683,289.60	639,206.40	595,123.20	551,040.00
75	688,537.60	667,020.80	623,987.20	580,953.60	537,920.00
50	671,744.00	650,752.00	608,768.00	566,784.00	524,800.00
25	654,950.40	634,483.20	593,548.80	552,614.40	511,680.00
10	638,156.80	618,214.40	578,329.60	538,444.80	498,560.00
90	528,998.40	512,467.20	479,404.80	446,342.40	413,280.00
75	516,403.20	500,265.60	467,990.40	435,715.20	403,440.00
50	503,808.00	488,064.00	456,576.00	425,088.00	393,600.00
25	491,212.80	475,862.40	445,161.60	414,460.80	383,760.00
10	478,617.60	463,660.80	433,747.20	403,833.60	373,920.00
90	352,665.60	341,644.80	319,603.20	297,561.60	275,520.00
75	344,268.80	333,510.40	311,993.60	290,476.80	268,960.00
50	335,872.00	325,376.00	304,384.00	283,392.00	262,400.00
25	327,475.20	317,241.60	296,774.40	276,307.20	255,840.00
10	319,078.40	309,107.20	289,164.80	269,222.40	249,280.00
90	132,249.60	128,116.80	119,851.20	111,585.60	103,320.00
75	129,100.80	125,066.40	116,997.60	108,928.80	100,860.00
50	125,952.00	122,016.00	114,144.00	106,272.00	98,400.00
25	122,803.20	118,965.60	111,290.40	103,615.20	95,940.00
10	119,654.40	115,915.20	108,436.80	100,958.40	93,480.00
90	44.08	42.71	39.95	37.20	34.44
75	43.03	41.69	39.00	36.31	33.62
50	41.98	40.67	38.05	35.42	32.80
25	40.93	39.66	37.10	34.54	31.98
10	39.88	38.64	36.15	33.65	31.16

Table 7. Risked volume at P25

Risk	90	75	50	25	10
90	643,399.68	623,293.44	583,080.96	542,868.48	502,656.00
75	628,080.64	608,453.12	569,198.08	529,943.04	490,688.00
50	612,761.60	593,612.80	555,315.20	517,017.60	478,720.00
25	597,442.56	578,772.48	541,432.32	504,092.16	466,752.00
10	582,123.52	563,932.16	527,549.44	491,166.72	454,784.00
90	482,549.76	467,470.08	437,310.72	407,151.36	376,992.00
75	471,060.48	456,339.84	426,898.56	397,457.28	368,016.00
50	459,571.20	445,209.60	416,486.40	387,763.20	359,040.00
25	448,081.92	434,079.36	406,074.24	378,069.12	350,064.00
10	436,592.64	422,949.12	395,662.08	368,375.04	341,088.00
90	321,699.84	311,646.72	291,540.48	271,434.24	251,328.00
75	314,040.32	304,226.56	284,599.04	264,971.52	245,344.00
50	306,380.80	296,806.40	277,657.60	258,508.80	239,360.00
25	298,721.28	289,386.24	270,716.16	252,046.08	233,376.00
10	291,061.76	281,966.08	263,774.72	245,583.36	227,392.00
90	120,637.44	116,867.52	109,327.68	101,787.84	94,248.00
75	117,765.12	114,084.96	106,724.64	99,364.32	92,004.00
50	114,892.80	111,302.40	104,121.60	96,940.80	89,760.00
25	112,020.48	108,519.84	101,518.56	94,517.28	87,516.00
10	109,148.16	105,737.28	98,915.52	92,093.76	85,272.00
90	40.21	38.96	36.44	33.93	31.42
75	39.26	38.03	35.57	33.12	30.67
50	38.30	37.10	34.71	32.31	29.92
25	37.34	36.17	33.84	31.51	29.17
10	36.38	35.25	32.97	30.70	28.42

Table 8. Risked volume at P10

Risk	90	75	50	25	10
90	596,951.04	578,296.32	540,986.88	503,677.44	466,368.00
75	582,737.92	564,527.36	528,106.24	491,685.12	455,264.00
50	568,524.80	550,758.40	515,225.60	479,692.80	444,160.00
25	554,311.68	536,989.44	502,344.96	467,700.48	433,056.00
10	540,098.56	523,220.48	489,464.32	455,708.16	421,952.00
90	447,713.28	433,722.24	405,740.16	377,758.08	349,776.00
75	437,053.44	423,395.52	396,079.68	368,763.84	341,448.00
50	426,393.60	413,068.80	386,419.20	359,769.60	333,120.00
25	415,733.76	402,742.08	376,758.72	350,775.36	324,792.00
10	405,073.92	392,415.36	367,098.24	341,781.12	316,464.00
90	298,475.52	289,148.16	270,493.44	251,838.72	233,184.00
75	291,368.96	282,263.68	264,053.12	245,842.56	227,632.00
50	284,262.40	275,379.20	257,612.80	239,846.40	222,080.00
25	277,155.84	268,494.72	251,172.48	233,850.24	216,528.00
10	270,049.28	261,610.24	244,732.16	227,854.08	210,976.00
90	111,928.32	108,430.56	101,435.04	94,439.52	87,444.00
75	109,263.36	105,848.88	99,019.92	92,190.96	85,362.00
50	106,598.40	103,267.20	96,604.80	89,942.40	83,280.00
25	103,933.44	100,685.52	94,189.68	87,693.84	81,198.00
10	101,268.48	98,103.84	91,774.56	85,445.28	79,116.00
90	37.31	36.14	33.81	31.48	29.15
75	36.42	35.28	33.01	30.73	28.45
50	35.53	34.42	32.20	29.98	27.76
25	34.64	33.56	31.40	29.23	27.07
10	33.76	32.70	30.59	28.48	26.37

Table 9 is a summary of Tables 4 to 8 under maximum (Max), minimum (Min) and average (Mean) at the different risk levels.

Table 9. Summarized risked hydrocarbon volume

Risk	Maximum (m^3)	Minimum (m^3)	Mean (m^3)
90	816,291.84	36.06	341,102.12
75	760,381.44	33.59	317,738.96
50	705,331.20	31.16	294,735.24
25	643,399.68	28.42	268,856.05
10	596,951.04	26.37	249,446.65

The maximum varies between about 597 thousand cubic metres at P10 and about 816 thousand cubic metres at P90. While the average values vary between about 249 thousand cubic metres at P10 and about 340 thousand cubic metres at P90. The minimum can be as low as 26.37 cubic metres at P10 and not more than 36 cubic metres at P90. There is a 90% chance of obtaining more than 26.37 cubic metres at P10 whereas there is only a 10% chance of obtaining more than 816 thousand cubic metres at P90. As it were, the volume risk is influenced greatly by the uncertainty in the combining parameters. These quantified associated uncertainties in the estimation of hydrocarbon volume characteristics can be used to provide optimal decision regarding future hydrocarbon extraction plan.

5 Conclusions

Reservoir volume risk has been assessed from a combination of well logs and seismic volume using multiple-point stochastic inversion procedure. A variety of reservoir parameter results obtained at different probability levels allow for the quantification of sufficient possibilities of risks for a robust hydrocarbon extraction plan

References

[1] Wang Y. Seismic Inversion – Theory and Applications. Wiley-Blackwell Publishing, Ltd., 2017; 257 pp.
[2] Francis AM. A simple guide to seismic inversion. GEO ExPro APRIL 2013; vol. 10, no. 2, pp 46 – 50.
[3] Zhang Y, Jiangwo Y, Fei L, Chao C, Bao M, Shuanggen J, James HD. A new bound constraints method for 3D Potential field data Inversion using Lagrangian Multipliers. Geophys. J. Int., 2015; 2(1): 267-275.
[4] Pendrel J. "Seismic Inversion—A Critical Tool in Reservoir Characterization", Scandinavian Oil-Gas Magazine, 2006; No. 5/6, p. 19-22.
[5] Bempong FK, Ehinola O, Apesegah E, Hotor VK, Botwe T. Sequence Stratigraphic Framework, Depositional Settings and Hydrocarbon Prospectivity of the Campanian Section, Tano Basin, Southwestern Ghana. Petroleum & Coal, 2021; 63(1): 204-215.
[6] Falebita DE, Olusanya AT, Akinsanpe OT. Analysis of Seismic Gas Chimney Distribution Using Artificial Neural Network – A Case of Shallow Offshore Field, Niger Delta, Nigeria. Petroleum & Coal, 2017; 59(6), 808-819.
[7] Heggland R, Nygaard E, Gallagher JW. Techniques and Experiences Using Exploration 3D Seismic Data to Map Drilling Hazards. Proceedings of Offshore Technology Conference,(OTC), Houston, 6 - 9, 1996; 1: 111 – 124.
[8] Gallagher JW and Heggland R. Shallow Gas Evaluations Based on Conventional 3D Seismic Data, 56th EAGE Meeting, June 6 - 10, 1994; Vienna, .
[9] Robinson G. Stochastic Seismic Inversion Applied To Reservoir Characterization. CSEG Recoder, January 01, 2001; pp 36-40.
[10] Hoffman BT and Caers J. Regional probability perturbations for history matching. Journal of Petroleum Science and Engineering, 2005; 46, 53– 71.
[11] Liu Y, Harding A, Abriel W and Strebelle S. Multiple-point Simulation Integrating Wells, 3-D Seismic and Geology. American Association of Petroleum Geologists Bulletin, 2004; 58(7): 905-921.
[12] Caers J, Strebelles S, and Payrazyan, K. Stochastic integration of seismic data and geologic scenarios – A West Africa submarine channel saga, Leading Edge, 2003; 23(3): 192-196.
[13] Strebelle S. Sequential Simulation – Drawing structures from training images. Unpublished Ph.D. Thesis, Department of Geological and Environmental Sciences, Standford University, USA, 2001; 200 p.
[14] Jenkins GF and Brown GM. Stochastic Inversion. SEG Expanded Abstract, 2000; pp 1 – 4.
[15] Francis AM. Deterministic Inversion: Overdue for Retirement? Presented at PETEX 2002 Conference and Exhibition, London, UK
[16] Francis AM. Stochastic seismic inversion: solving large problems. Presented at IAMG 2003 Conference, Portsmouth, UK
[17] Pardo-Iguzquiza E and Chica-Olmo. The Fourier integral method: An efficient spectral method for simulation of random fields. Mathematical Geology, 1993; 25 (4): 177-217.
[18] Doust H and Omatsola E. Niger Delta, in J. D. Edwards, and P. A. Santogrossi, eds., Divergent/passive margins basins: AAPG Memoir 1990; 48: 201–238.
[19] Whiteman A. Nigeria – its petroleum geology, resources and potential, London, Graham and Trotman, 1982; 394 p.
[20] Burke K. Longshore drift, submarine canyons and submarine fans in development of Niger Delta: American Association of Petroleum Geologists Bulletin, 1972; 56: 1975-1983.
21[] Petroleum Inspectorate (Nigeria). Standardization of Geological Nomenclature and Symbols, 1985; pp 19.
[22] Evamy BD, Haremboure J, Knaap P, Molloy FA and Rowlands PH. Hydrocarbon Habitat of Tertiary Niger Delta, American Association of Petroleum Geologists Bulletin, 1978; 62, 1-39.
[23] EWManual. MPSI™: Plugin to OpendTect. Earthworks Environment & Resources Ltd and Ark-CLS, 2010; 141 p. http://www.sorviodvnvm.co.uk; http://www.arkcls.com/
[24] Gringarten E and Deutsch CV. Variogram Modelling and Interpretation, Mathematical Geology, 2001; 33(4): 507-534.
[25] Ivits-Wasser E. "Potential of remote sensing and GIS as landscape structure and biodiversity indicators", Albert-Ludwigs-Universität Freiburg i. Brsg. Freiburg i. Brsg. 2004; 232 pp.
[26] Francis AM. Limitations of Deterministic and Advantages of Stochastic Seismic Inversion. CSEG Recorder, February, 2005; pp 1 – 11.

[27] Dubrule O. Geostatistics for Seismic Data Integration in Earth Models. Distinguished Instructor Short Course, Series 6; Society of Exploration Geophysicists & European Association of Geoscientists and Engineers, 2003; 1-1: 11-10.
28[] Goovaerts P. Geostatistics for Natural Resources Evaluation. Applied Geostatistics Series. Oxford University Press, New York, 1997; 483 p.
[29] Short KC and Stauble AJ. Outline of geology of Niger Delta. Am Asso Petrol Geol Bull, 1967; 51:761–779

To whom correspondence should be addressed: Dele Falebita, Department of Geology, Obafemi Awolowo University, Ile-Ife, Nigeria, E-mail: delefale@oauife.edu.ng